Princeton Plasma Physics Laboratory

PPPL- 4299

PPPL- 4299

New Capabilities and Results for the National Spherical Torus Experiment

M.G. Bell, R.E. Bell, D.A. Gates, S.M. Kaye, H. Kugel, B.P. LeBlanc, F.M. Levinton, R. Maingi, J.E. Menard, R. Raman, S.A. Sabbagh, D. Stutman and the NSTX Research Team

February 2008

Prepared for the U.S. Department of Energy under Contract DE-AC02-76CH03073.

Princeton Plasma Physics Laboratory
Report Disclaimers

Full Legal Disclaimer

This report was prepared as an account of work sponsored by an agency of the United States Government. Neither the United States Government nor any agency thereof, nor any of their employees, nor any of their contractors, subcontractors or their employees, makes any warranty, express or implied, or assumes any legal liability or responsibility for the accuracy, completeness, or any third party's use or the results of such use of any information, apparatus, product, or process disclosed, or represents that its use would not infringe privately owned rights. Reference herein to any specific commercial product, process, or service by trade name, trademark, manufacturer, or otherwise, does not necessarily constitute or imply its endorsement, recommendation, or favoring by the United States Government or any agency thereof or its contractors or subcontractors. The views and opinions of authors expressed herein do not necessarily state or reflect those of the United States Government or any agency thereof.

Trademark Disclaimer

Reference herein to any specific commercial product, process, or service by trade name, trademark, manufacturer, or otherwise, does not necessarily constitute or imply its endorsement, recommendation, or favoring by the United States Government or any agency thereof or its contractors or subcontractors.

PPPL Report Availability

Princeton Plasma Physics Laboratory:

http://www.pppl.gov/techreports.cfm

Office of Scientific and Technical Information (OSTI):

http://www.osti.gov/bridge

Related Links:

U.S. Department of Energy

Office of Scientific and Technical Information

Fusion Links

New Capabilities and Results for the National Spherical Torus Experiment

M.G. Bell, R.E. Bell, D.A. Gates, S.M. Kaye, H. Kugel, B.P. LeBlanc, F.M. Levinton[1], R. Maingi[2], J.E. Menard, R. Raman[3], S.A. Sabbagh[4], D. Stutman[5] and the NSTX Research Team[6]

Plasma Physics Laboratory[*]*, Princeton University, PO Box 451, Princeton, NJ 08543, USA*
Author's email: MBell@pppl.gov[‡]

Abstract

The National Spherical Torus Experiment (NSTX) produces plasmas with toroidal aspect ratio as low as 1.25, which can be heated by up to 6 MW High-Harmonic Fast Waves and up to 7 MW of deuterium Neutral Beam Injection. Using new poloidal fields coils, plasmas with cross-section elongation up to 2.7, triangularity 0.8, plasma currents I_p up to 1.5 MA and normalized currents $I_p/a{\cdot}B_T$ up to 7.5 MA/m·T have been achieved. A significant extension of the plasma pulse length, to 1.5 s at a plasma current of 0.7 MA, has been achieved by exploiting the bootstrap and NBI-driven currents to reduce the dissipation of poloidal flux. Inductive plasma startup has been supplemented by Coaxial Helicity Injection (CHI) and the production of persistent current on closed flux surfaces by CHI has now been demonstrated in NSTX. The plasma response to magnetic field perturbations with toroidal mode numbers n = 1 or 3 and the effects on the plasma rotation have been investigated using three pairs of coils outside the vacuum vessel. Recent studies of both MHD stability and of transport benefitted from improved diagnostics, including measurements of the internal poloidal field using the motional Stark effect (MSE). In plasmas with a region of reversed magnetic shear in the core, now confirmed by the MSE data, improved electron confinement has been observed.

1. Introduction

The National Spherical Torus Experiment (NSTX) produces plasmas with toroidal aspect ratio as low as 1.25, which can be heated by up to 6 MW High-Harmonic Fast Waves (HHFW) and 7 MW of deuterium Neutral Beam Injection (NBI). Conducting plates surround the plasma on the outside to provide stabilization against pressure-driven modes. The device has been described in reference [1] and results through 2004 have been discussed in reference [2].

In 2005, NSTX completed 18 weeks of operation, providing data for some 38 separate experiments. The toroidal field coil, which had undergone refurbishment of its bolted joints at

---

[1] Nova Photonics, Princeton, New Jersey, USA
[2] Oak Ridge National Laboratory, Oak Ridge, Tennessee, USA
[3] University of Washington, Seattle, Washington, USA
[4] Columbia University, New York, New York, USA
[5] Johns Hopkins University, Baltimore, Maryland, USA
[6] See Appendix for members of the NSTX Team
[*] Work supported by U.S. Department of Energy Contract DE-AC02-76CH03073
[‡] This is a preprint of an article to be published in the journal Nuclear Fusion, a publication of the International Atomic Energy Agency (http://www.iop.org/ej/nf).

the conclusion of the 2004 experiments, operated for about 2500 pulses. At the end of the operating period, the coil was run up to 95% of its design rating of 0.6 T (at the nominal radius of 0.85 m), although the majority of experiments were conducted with fields up to 0.45 T. Throughout the 2005 operation, the measured resistances of the 72 joints in the coil remained well within specifications and did not show evidence of significant deterioration.

Several new capabilities were introduced during 2005. In particular, recent NSTX experiments have benefitted from measurements of the internal poloidal field at eight points along the plasma minor radius using the motional Stark effect (MSE) on collisionally excited emission from the deuterium NBI [3]. The successful application of the MSE technique in the low magnetic field typical of NSTX represents a major achievement in diagnostic development. The MSE data are used as constraints in the analysis of the plasma equilibrium with the EFIT code, which can also include kinetic profiles, including the electron pressure measured by Thomson scattering and the thermal ion pressure and toroidal rotation measured by charge-exchange recombination spectroscopy (CHERS) [4]. In the following sections, some of the other new capabilities of NSTX will be described and selected highlights of experimental results will be presented.

2. Improvements in Plasma Shaping Capability and the Effects on Plasma Stability

Prior to the 2005 experiments, the two innermost poloidal field coils at the upper and lower ends of the central solenoid, known as the PF1A coils, were replaced by an axially shorter pair further from the midplane to increase the plasma shaping, in particular the capability to produce simultaneously high elongation, κ, and triangularity, δ, of the plasma cross-section. Plasmas with $\kappa = 2.7$ and $\delta_{av} = 0.8$ (where δ_{av} is the average of the upper and lower triangularity) have now been produced at an aspect ratio A = 1.5. The changes in the coils and representative plasma shapes are shown in Fig. 1. Comparisons of the values of κ and δ_{av} achieved in 2004 and 2005 are shown in Fig. 2. The highest value of the "shaping factor" $q_{95}I_p/aB_T$ (where q_{95} is the safety factor at the 95% normalized flux surface, I_p the plasma current, a the mid-plane half-width of the cross-section and B_T the vacuum toroidal magnetic field at the plasma geometric center) reached 37 MA/m·T at a slightly lower aspect ratio A = 1.35 with $\kappa = 2.3$, $\delta = 0.6$ [5]. Plasma currents I_p up to 1.5 MA have now been achieved. At an applied toroidal field of 0.45 T, the plasma stored energy reached 430 kJ, a record for NSTX, for a NBI heating power of 7.3 MW. At lower field, 0.34 T, the toroidal beta, β_T, reached 35% in 2005 operation, although maximizing β_T was not a major focus of the experiments in 2005. By ramping down the plasma current during NBI, poloidal-beta, β_P, up to 2.1 and Troyon-normalized beta $\beta_N = \beta_T/(I_p/aB_T)$ up to 7.2 %·m·T/MA have been produced, which significantly exceed the ideal stability limit calculated without wall stabilization.

One result of operating with higher κ and δ simultaneously was the re-emergence of small, high-frequency ELMs [6] in H-mode plasmas. Previously, operating at $\kappa > 2.2$ with lower triangularity produced large ELMs, each of which caused a significant drop in the plasma energy. The small ELMs do not individually perturb the plasma energy significantly. Despite this, the enhancement factor of the global energy confinement time relative to both the ITER-L97 and the ITER-H98pb(y,2) scalings [7] actually decreased slightly with increasing

κ, as discussed in ref. [8]. The small ELMs are, however, effective in slowing the rate of density rise, which has enabled a significant extension in the pulse length achievable at moderate plasma currents, 0.7 – 1.0 MA. Figure 3 shows basic waveforms for a lower single-null divertor (LSND) discharge which extended to 1.5 s at 0.7 MA; the current was constant for about 4 current-relaxation times. Calculations have been made with the TRANSP code [9] of the non-inductively driven current in this plasma assuming classical thermalization of the energetic ions introduced by NBI; this assumption provides a good match between the measured and predicted DD fusion neutron rates. As seen in Fig. 4, the calculation shows that the non-inductive components, including the neoclassical bootstrap current [10], other ∇p terms and the beam-driven current, provide up to 70% of the total current at peak β. Despite the beneficial effect of the ELMs in slowing the density rise, this discharge reached the nominal Greenwald density limit (Fig. 3, bottom panel). This roughly coincided with a drop in the central rotation of the plasma, the development of a persistent saturated n=1 mode and a drop in β. While this coincidence may not indicate causality, it does indicate that density control will be a major issue for the development of even longer H-mode discharges in NSTX. This discharge did not utilize the full flux swing available from the transformer but suffered a final MHD-related collapse at the end of the NBI pulse when the central safety factor q(0) had reached 1. A small extension of the pulse length over previous results was also obtained at a higher plasma current, 1.0 MA, in a double-null divertor discharge with $\kappa = 2.3$, $\delta_{av} = 0.6$.

4. Generation of Persistent Toroidal Current by Coaxial Helicity Injection

Coaxial Helicity Injection has the potential to initiate toroidal plasma current in the ST by creating a discharge and injecting poloidal current from electrodes coaxial with the major axis in the presence of applied toroidal and appropriate poloidal magnetic fields. Recent experiments in NSTX have aimed to exploit the technique of "transient CHI" originally developed in the HIT-II device [11]. The NSTX experiments in 2005 benefitted from several upgrades, including the capability to inject both the gas and the ECRF (18 GHz) microwave power for initiating the discharge directly into the chamber below the CHI electrodes. This reduced the gas needed to create the discharge, thereby increasing the energy input per particle and thus the possible temperature of the CHI discharge in its high-current phase. A fast "crowbar" switch was also provided for the capacitor bank supply (10 – 50 mF, 2 kV rated) so that the injected current could be reduced rapidly once the CHI discharge had expanded to fill the region available for plasma inside the vacuum vessel. With these changes, a clear demonstration was obtained of toroidal plasma current which persisted on closed magnetic surfaces beyond the end of the injector current pulse. Fig. 5 shows examples of the discharge waveforms for a shot obtained with a 15 mF capacitor bank charged to 1.5 kV in which a peak toroidal plasma current of 120 kA was generated for an injected current of 1.9 kA, representing a current multiplication factor greater than 60. When the injector current had decayed to zero ($t \approx 11$ ms), approximately 6.5 kJ of electrical energy had been dissipated in the plasma circuit. At this time, a toroidal plasma current of 50 kA was still flowing, which subsequently decayed on a timescale of about 7 ms. Images of the visible light emission during this phase showed the formation of a plasma ring detached from the injector and close

to the center column. Further details of these results are given in reference [12]. Future experiments will attempt to maximize the CHI-initiated current and to couple these discharges both to inductive and non-inductive current drive.

3. Effects of Applied Radial Field Perturbations on Plasma Stability and Rotation

NSTX routinely operates with normalized-beta above the stability limit calculated without the stabilizing effect of the conducting wall, so plasmas are susceptible to the growth of resistive wall modes (RWM) unless sufficient plasma rotation can be maintained. Non-axisymmetric field perturbations, both intrinsic and induced by the modes themselves, can act to slow the rotation induced by the NBI heating in NSTX and thereby contribute to mode growth. To allow extended operation near the ideal-wall limits, three pairs of nearly rectangular coils have been installed on the mid-plane outside the vacuum vessel to produce radial magnetic field perturbations. Each coil has an area of about 1.6 m^2 and contains two turns, The diametrically opposite coil pairs are powered by three power amplifiers, which can drive currents up to 3 kA at frequencies up to several kHz.

The effect of DC perturbations generated by the coils with toroidal mode number n = 1 on the development of locked modes was investigated first; the results are summarized in Fig. 6. In a series of otherwise similar ohmically heated, low-density, deuterium, LSND plasmas, the amplitude of the applied perturbation at the inferred q = 2 surface needed to trigger a locked mode as a function of its direction, traced out a circle, suggesting that there is an intrinsic radial error field perturbation corresponding to the vector from the center of the circle to the origin, *i.e*. about 1.3 Gauss in the conditions of these discharges.

The response to stationary perturbations with toroidal mode numbers n = 1 or 3 has also been investigated in initially rapidly rotating plasmas heated by 6 MW of NBI to $\beta_N \approx 5$. As seen in Fig. 7, when a small n = 1 perturbation was applied in the direction to augment the intrinsic error field, the plasma toroidal rotation (measured by CHERS) collapsed, starting near the edge but then extending across the profile. A locked mode then developed and the discharge terminated earlier than a reference shot with no perturbation. Conversely, when the applied perturbation counteracted the intrinsic error field, the rotation collapse was avoided and the high-β_N phase was extended. When a 50 ms long, n = 3 perturbation pulse was applied to a similar NBI-heated discharge, the plasma rotation at the edge stopped temporarily but, provided that a locked mode not develop while the plasma edge was stationary, resumed after the perturbation was removed. In this case, the perturbation of toroidal rotation in the plasma center, which did not contain q-surfaces resonant with the applied n = 3 perturbation, appeared to be damped by neoclassical toroidal viscosity [13,14].

5. Use of Lithium Coating to Control Recycling from Plasma Facing Surfaces

The Lithium Pellet Injector [15], first introduced in 2004 [16], has been used to produce changes in the recycling of hydrogenic species from the plasma contact surfaces, which contributes to the secular density rise observed in most NBI-heated plasmas in NSTX. The experiments involved both plasmas limited on the central column and lower single-null

divertor plasmas; both these contact areas are covered by carbon tiles. For each configuration, the surface layers of the plasma contact area were first depleted of deuterium by a series (~10) of low-density, ohmically heated, helium discharges. These were followed by a reference deuterium discharge with 2 MW of NBI heating. One or two lithium pellets with masses 1.7 – 5 mg were then injected into each of a series (10 – 20) of helium discharges, to introduce a total of 24 – 30 mg of lithium. Spectroscopic data indicated that the injected lithium was deposited primarily on the surfaces surrounding the plasma contact area. In both the limiter and divertor configurations, the first subsequent deuterium NBI-heated plasma showed a reduction in the volume-average plasma density during the NBI heating by a factor of about 2 compared to the respective reference discharge before the lithium deposition. This reduction in density was less on the next shot and was not evident on the third shot. This is illustrated for the divertor configuration plasmas in Fig. 8. The saturation of the apparent wall pumping can be understood if the effect occurs through the formation of lithium deuteride on the surface: the amount of lithium introduced could react with about 6 – 9 mg of deuterium and about 3.5 mg of deuterium was injected on each discharge. The lithium deposition was repeated for the plasmas limited on the central column, without any preceding helium-only sequence, and a similar reduction in density was observed on the first subsequent NB-heated shot. The results for the limiter plasmas are similar to the experience with lithium coating in TFTR [17] and with a liquid-lithium limiter in CDX-U [18], but these NSTX experiments extend the potential benefits of lithium surface coating for plasma density control to divertor plasmas.

5. Effect of Modifying the Magnetic Shear on Electron Thermal Transport

As previously reported [19], with NBI heating, the confinement of both the thermal and unthermalized ions is extremely good in NSTX and, in most operating regimes, the dominant thermal loss is through the electron channel. However, in plasmas with a fast initial current ramp which develop a region of strongly reversed magnetic shear in the core, improved electron confinement has also been observed [20]. The creation of reversed shear in these discharges was previously inferred from the behavior of perturbations on the soft x-ray emission profiles, supported by TRANSP modeling of the current diffusion assuming neoclassical plasma resistivity. The MSE measurements of the q-profile made this year have confirmed the inference of reversed shear and also guided the development of a scenario for obtaining reversed magnetic shear reliably.

Fig. 9a shows the waveforms for two successive discharges with a flattop current of 1MA but slightly different initial current ramps and timing of the NBI, while Fig. 9b shows the resultant q-profiles at t = 0.3s as determined by the LRDFIT code using the MSE pitch-angle data as a constraint on the fit. The production of strongly reversed shear through a fast current ramp is very sensitive to the MHD mode activity in the ramp-up phase of the discharge: quite small bursts of activity detected by the Mirnov coils can be accompanied by a rapid drop in the central q and result in a profile with weak negative or near-zero shear in the center. However, once established, a strongly reversed-shear profile can be maintained for up to 0.2s

A comparison of the profiles of the plasma temperatures and density is shown in Fig. 10a. Although the ion temperature is very similar in the two discharges, the electron temperature is significantly higher in the strongly reversed-shear case, suggesting a reduction in electron thermal transport, which has been confirmed by TRANSP analysis, again based on classical thermalization of the fast ions from NBI. The electron thermal diffusivities calculated by TRANSP for the two discharges are shown in Fig. 10b; a reduction of χ_e by a factor 2 – 4 over the inner 70% of the minor radius is evident. Adding a modest amount of HHFW heating power, ~0.7 MW, launched with balanced $k_{||} \approx \pm 7$ m^{-1} produced measurable electron heating in the central region of a reversed-shear plasma established with 2 MW of NBI.

6. Summary and Plans

With new capabilities and reliable operation of the facility, NSTX completed a productive period of experiments in 2005 which have extended its operating regime in several directions. The new inner poloidal field coils have produced plasmas with simultaneously high κ and δ, resulting in the achievement of a record plasma stored energy of 430 kJ. Small ELMs are observed in high-κ, high-δ H-mode plasmas; this regime has provided a route to extend the pulse length significantly in NSTX, to 1.5 s at 0.7 MA and 1.0 s at 1.0 MA. Transient CHI has produced closed flux surfaces carrying a toroidal current up to about 50kA. The error-field correction coils have been used to cancel intrinsic error fields, thereby delaying the growth of locked modes and extending the pulse length at high-β_N. Braking of plasma rotation by applied field perturbations has been demonstrated. Injection of lithium pellets into helium plasmas has been used to coat the plasma contact surfaces with lithium, which has then provided edge pumping of deuterium and plasma density control until the lithium becomes saturated. The production of reversed shear in plasmas with a fast initial current ramp has been confirmed by MSE measurements of the q-profile; these plasmas have shown reductions in electron thermal transport by a factor 2 – 4 compared to similar discharges with weakly negative or positive shear. It will be particularly interesting to study this regime with a tangential microwave scattering diagnostic now being commissioned on NSTX designed to detect fluctuations with radial wavenumbers in the range $k_r = 2 - 22$ cm^{-1} thought to be important in producing electron transport.

Following the experiments in 2005, NSTX began an outage period during which preparations were made to install a lithium evaporator for coating the plasma contact surfaces with more copious amounts of lithium than are possible through pellet injection. Operation of NSTX is planned to resume early in 2006.

Acknowledgements

This paper reports the results of experiments prepared, conducted and analyzed by a dedicated team of researchers, engineers and support staff from PPPL and several collaborating institutions. Their efforts and contributions to this paper are gratefully acknowledged. This work is supported by US Department of Energy Contract DE-AC02-76CH03073 and other contracts with the collaborating institutions.

References

[1] Ono, M. *et al.*, Nucl. Fusion **40** (2000) 557.

[2] Kaye, S.M. *et al.*, Nucl. Fusion **45** (2005) S168.

[3] Levinton, F.M. *et al.*, Phys. Rev. Lett. **63** (1989) 2060.

[4] Sabbagh, S.A. *et al.*, Nucl. Fusion **41** (2001) 1601.

[5] Gates, D.A. *et al.*, "The effect of plasma shaping on plasma performance in the NSTX", *submitted for publication in Phys. Plasmas.*

[6] Maingi, R. *et al.*, Nucl. Fusion **45** (2005) 264.

[7] ITER Physics Expert Groups, Nucl. Fusion **39** (1999) 2175.

[8] Kaye, S.M. *et al.*, "Energy Confinement Scaling in the Low Aspect Ratio National Spherical Torus Experiment (NSTX)", *submitted for publication in Nucl. Fusion.*

[9] Kaye, S.M. *et al.*, Phys. Plasmas **10** (2003) 3953.

[10] Houlberg W.A. *et al.* Phys. Plasmas **4** (1997) 3230.

[11] Raman, R. *et al.*, Phys. Rev. Lett., 075005-1 (2003).

[12] Raman, R. *et al.*, "Solenoid-free Plasma Startup in NSTX using Transient CHI", *submitted to Phys. Rev. Lett.*

[13] Sontag, A.C., Sabbagh, S.A., Zhu, W., Phys. Plasmas **12** (2005) 056112.

[14] Shaing, K.C., Phys. Plasmas **11** (2004) 5525.

[15] Gettelfinger, G. *et al.* Proc. 20th IEEE/NPSS Symposium on Fusion Engineering, San Diego CA, Oct. 14–17, 2003 (IEEE, Piscataway NJ 2003), p. 359.

[16] Kugel, H.W. *et al.*, "Initial NSTX Lithium Pellet Injection", poster JP1.007, presented at 46th Annual Meeting, Division of Plasma Physics, American Physical Society, Savannah GA, Nov. 2004, Bull. Am. Phys. Soc. **49** (8) (2004) 221.

[17] Mansfield, D.K., *et al.*, Phys. Plasmas **3**, (1996) 1892.

[18] Kaita, R. *et al.*, J. Nucl. Materials **337-339** (2005) 872.

[19] Gates, D.A. *et al.*, Phys. Plasmas **10** (2003) 1659.

[20] Stutman, D. "An assessment of electron thermal transport dynamics and its origins on NSTX", *to be published.*

Appendix: Members of the NSTX Research Team

M.G. Bell, R.E. Bell, S. Bernabei, J.M. Bialek[1], T. Bigelow[2], M. Bitter, T.M. Biewer[3], W. Blanchard, J. Boedo[4], C. Bush[2], J. Chrzanowski, D.S. Darrow, L. Dudek, R. Feder, J.R. Ferron[5], J. Foley[6], E.D. Fredrickson, D.A. Gates, G. Gettelfinger, T. Gibney, R. Harvey[7], R. Hatcher, W. Heidbrink[8], T.R. Jarboe[9], D.W. Johnson, M. Kalish, R. Kaita, S.M. Kaye, C. Kessel, S. Kubota[10], H.W. Kugel, G. Labik, B.P. LeBlanc, K.C. Lee[11], F.M. Levinton[6], D. Liu[8], J. Lowrance[12], R. Maingi[2], J. Manickam, R. Maqueda[6], R. Marsala, D. Mastrovito, E. Mazzucato, S.S. Medley, J. Menard, M. Ono, D. Mueller, T. Munsat[13], B.A. Nelson[9], C.L. Neumeyer, N. Nishino[14], H.K. Park, S.F. Paul, T. Peebles[10], E. Perry, Y-K.M. Peng[2], C.K. Phillips, R. Pinsker[5], S. Ramakrishnan, R. Raman[9], P. Roney, A.L. Roquemore, P.M. Ryan[2], S.A. Sabbagh[1], H. Schneider, C.H. Skinner, D.R. Smith, A.C. Sontag[1], V. Soukhanovskii[15], T. Stevenson, D. Stotler, B.C. Stratton, D. Stutman[16], D.W. Swain[2], E. Synakowski, Y. Takase[17], G. Taylor, K.L. Tritz[16], A. vonHalle, J. Wilgen[2], M. Williams, J.R. Wilson, I. Zatz, W. Zhu[1], S.J. Zweben, R. Akers[18], P. Beiersdorfer[15], P.T. Bonoli[3], C. Bourdelle[19], M.D. Carter[2], C.S. Chang[20], W. Choe[21], W. Davis, S.J. Diem, C. Domier[12], R. Ellis, P.C. Efthimion, A. Field[18], M. Finkenthal[16], E. Fredd, G.Y. Fu, A. Glasser[22], R.J. Goldston, L.R. Grisham, N. Gorelenkov, L. Guazzotto[23], R.J. Hawryluk, P. Heitzenroeder, K.W. Hill, W. Houlberg[2], J.C. Hosea, D. Humphreys[5], C. Jun, J.H. Kim[21], S. Krasheninnikov[4], L.L. Lao[5], S.G. Lee[24], J. Lawson, N.C. Luhmann[12], T.K. Mau[4], M.M. Menon[2], O. Mitarai[25], M. Nagata[26], D. Pacella[27], R. Parsells, A. Pigarov[4], G.D. Porter[15], A.K. Ram[3], D. Rasmussen[2], M. Redi, G. Rewoldt, E. Ruskov[8], I. Semenov[28], K. Shaing[29], K. Shinohara[30], M. Schaffer[5], P. Sichta, X. Tang[22], J. Timberlake, M. Wade[2], W.R. Wampler[31], R. Woolley, G.A. Wurden[22], X. Xu[15]

Princeton Plasma Physics Laboratory, Princeton University, New Jersey, USA

[1] *Columbia University, New York, New York, USA*
[2] *Oak Ridge National Laboratory, Oak Ridge, Tennessee, USA*
[3] *Massachusetts Institute of Technology, Cambridge, Massachusetts, USA*
[4] *University of California, San Diego, California, USA*
[5] *General Atomics, San Diego, California, USA*
[6] *Nova Photonics, Princeton, New Jersey, USA*
[7] *Compx, Del Mar, California, USA*
[8] *University of California, Irvine, California, USA*
[9] *University of Washington, Seattle, Washington, USA*
[10] *University of California, Los Angeles, California, USA*
[11] *University of California, Davis, California, USA*
[12] *Princeton Scientific Instruments, Princeton, New Jersey, USA*
[13] *University of Colorado, Boulder, Colorado, USA*
[14] *Hiroshima University, Hiroshima, Japan*
[15] *Lawrence Livermore National Laboratory, Livermore, California, USA*
[16] *Johns Hopkins University, Baltimore, Maryland, USA*
[17] *Tokyo University, Tokyo, Japan*
[18] *Euratom-UKAEA Fusion Association, Abingdon, Oxfordshire, United Kingdom*
[19] *CEA Cadarache, France*
[20] *New York University, New York, New York, USA*
[21] *Korea Advanced Institute of Science and Technology, Taejon, Republic of Korea*

[22] *Los Alamos National Laboratory, Los Alamos, New Mexico, USA*
[23] *University of Rochester, Rochester, New York, USA*
[24] *Korea Basic Science Institute, Taejon, Republic of Korea*
[25] *Kyushu Tokai University, Kumamoto, Japan*
[26] *Himeji Institute of Technology, Okayama, Japan*
[27] *ENEA, Frascati, Italy*
[28] *Kurcahtov Institute, Russia*
[29] *University of Wisconsin, Wisconsin, USA*
[30] *JAERI, Naka, Japan*
[31] *Sandia National Laboratories, Albuquerque, New Mexico, USA*

Figure Captions

Fig. 1 Cross-section through NSTX showing the PF1A coils (circled) and typical plasma configurations available in 2004 (left) and 2005 (right).

Fig. 2 Values of the plasma cross-section elongation κ and the triangularity δ_{av} averaged between the upper and lower X-points at the time of maximum β_T for discharges in which β_T exceeded 20%. Data from 2005 with the modified inner PF coils and from previous years are distinguished.

Fig. 3 Waveforms of discharge parameters for the longest duration 0.7MA plasma. The bottom panel shows the line-averaged density normalized to the limit predicted by Greenwald scaling.

Fig. 4 Results of TRANSP analysis for the plasma in Fig. 3 showing the time evolution of the measured and simulated DD neutron rates and the components of the total current

Fig. 5 Waveforms for a CHI discharge which produced a toroidal current of about 50kA as the injector current returned to zero. The toroidal current persisted for a further 10ms.

Fig. 6 Measurements of the threshold in the applied n=1 error field to generate a locked mode in otherwise similar plasmas as the direction of the applied field was varied. The error-field components are calculated at the inferred q = 2 surface, located at a normalized minor radius r/a = 0.6 – 0.7 at the mode onset.

Fig. 7 a) Waveforms for similar discharges with no applied error-field correction and with an n=1 error field applied in both the augmenting and canceling directions with respect to the intrinsic field;
b,c) Profiles of the toroidal rotation frequency ($=v_\phi/2\pi R$ measured by CHERS) at various times as the n=1 error field is applied in the augmenting (b) and canceling (c) directions.

Fig. 8 Waveforms of the plasma volume average density (calculated from the Thomson scattering profiles) for a reference NBI-heated deuterium discharge before deposition of lithium on the plasma contact surfaces, and for the first three similar discharges after depositing 25mg of lithium in a series of helium ohmically heated plasmas.

Fig. 9 a) Comparison of discharge waveforms for successive plasmas, the first developing a region of weakly, the second of strongly reversed shear; b) q-profiles for the two discharges at t = 0.31 s from analysis of the MSE data with the LRDFIT code.

Fig. 10 a) Profiles of the plasma temperatures and density for the two discharges in Fig. 9 at the times of peak plasma energy;
b) Profiles of the electron thermal diffusivity calculated by TRANSP (the bands indicate the variability of the diffusivity over the time interval indicated).

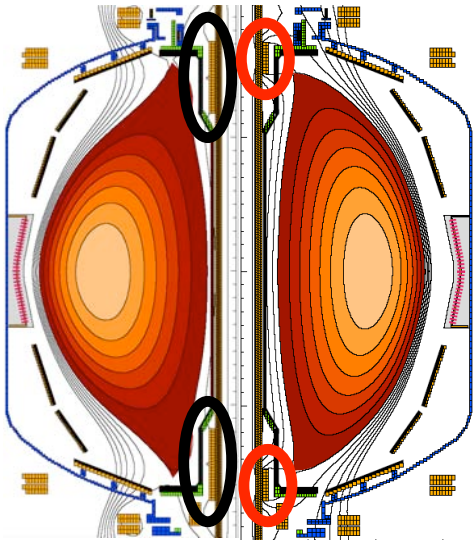

Fig. 1Cross-section through NSTX showing the PF1A coils (circled) and typical plasma configurations available in 2004 (left) and 2005 (right).

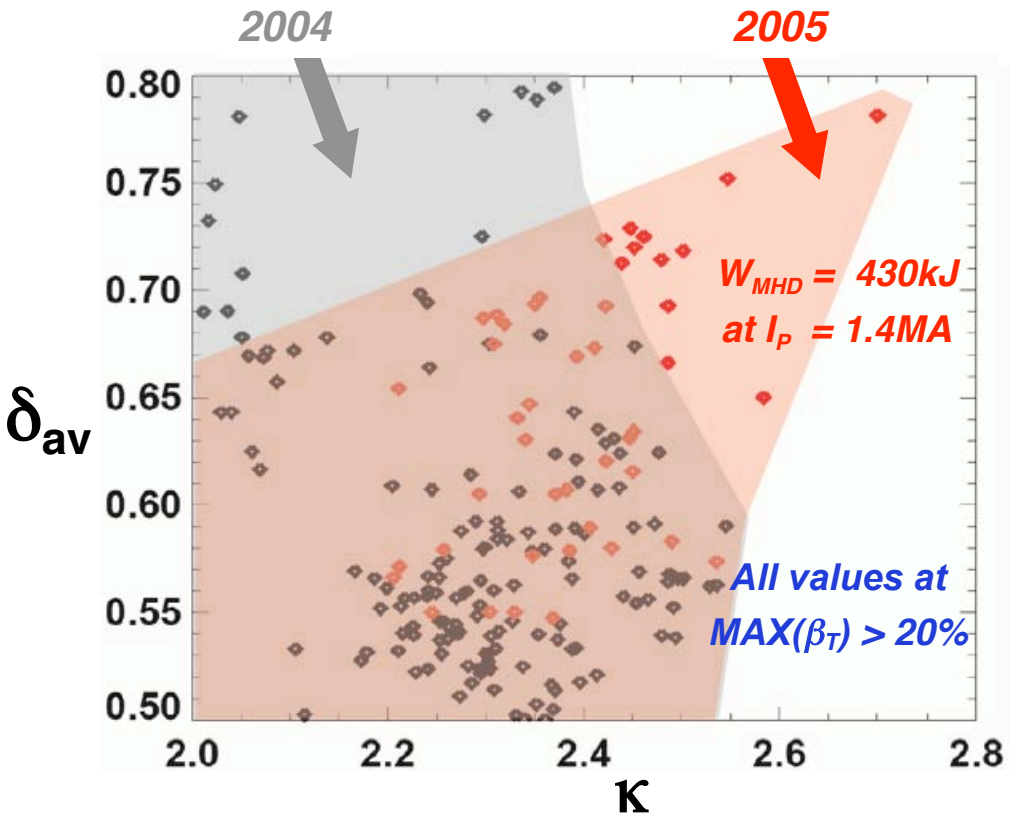

Fig. 2 Values of the plasma cross-section elongation κ and the triangularity δ_{av} averaged between the upper and lower X-points at the time of maximum β_T for discharges in which β_T exceeded 20%. Data from 2005 with the modified inner PF coils and from previous years are distinguished.

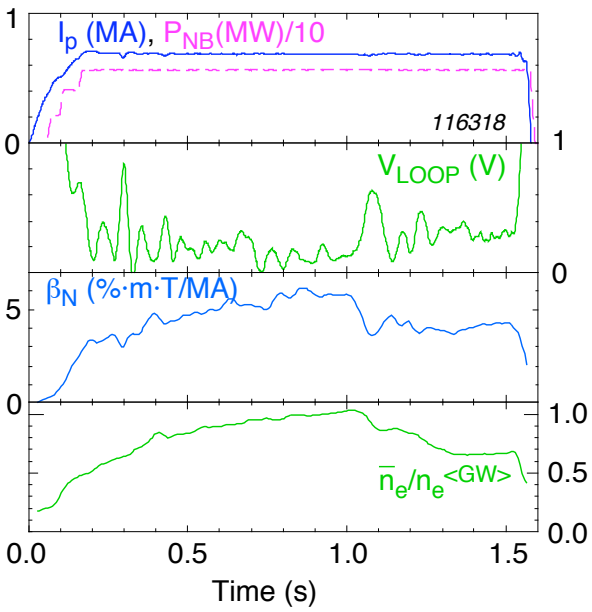

Fig. 3 Waveforms of discharge parameters for the longest duration 0.7MA plasma. The bottom panel shows the line-averaged density normalized to the limit predicted by Greenwald scaling.

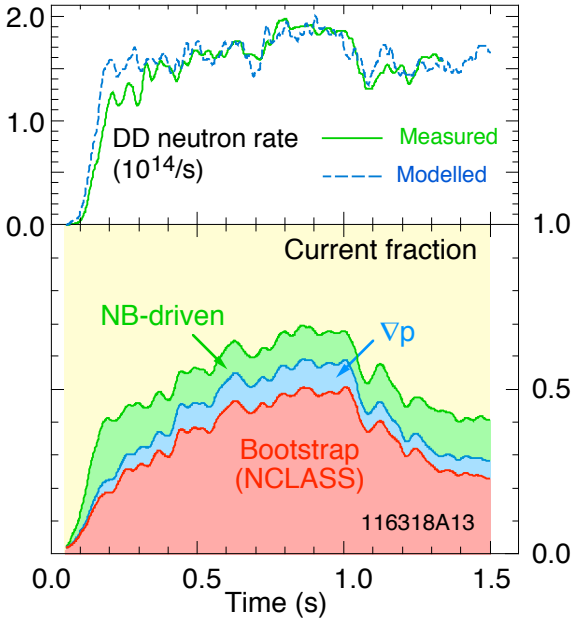

Fig. 4 Results of TRANSP analysis for the plasma in Fig. 3 showing the time evolution of the measured and simulated DD neutron rates and the components of the total current.

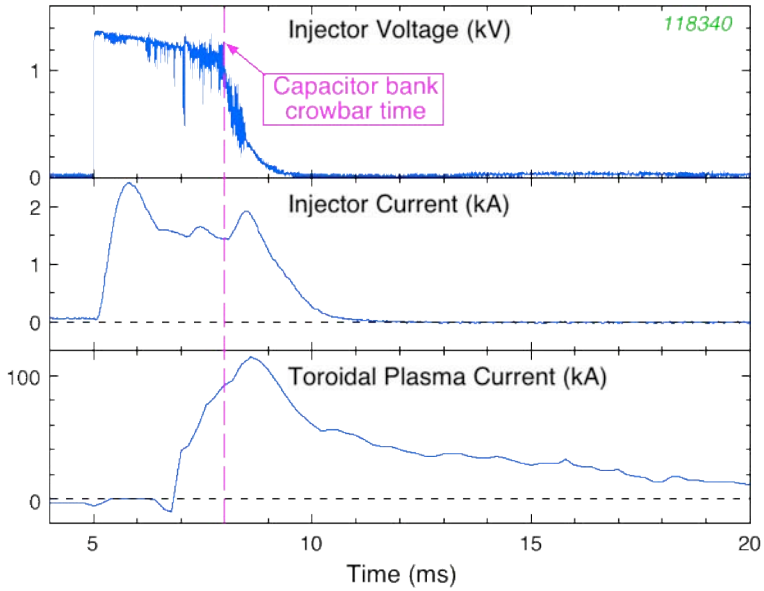

Fig. 5 Waveforms for a CHI discharge which produced a toroidal current of about 50kA as the injector current returned to zero. The toroidal current persisted for a further 10ms.

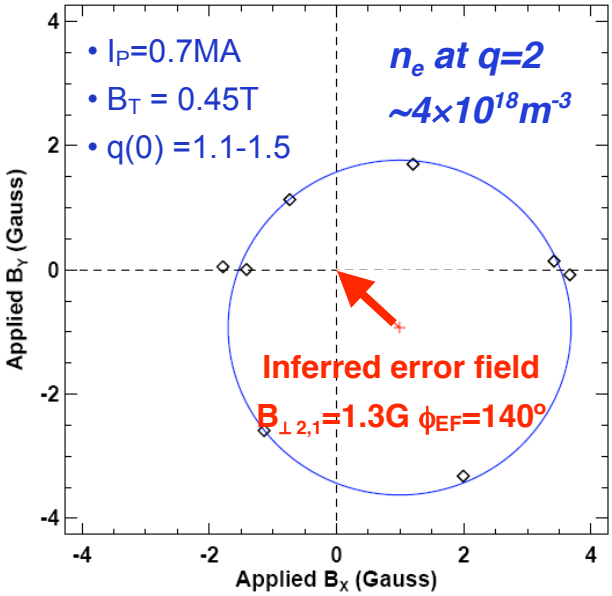

Fig. 6 Measurements of the threshold in the applied n=1 error field to generate a locked mode in otherwise similar plasmas as the direction of the applied field was varied. The error-field components are calculated at the inferred q = 2 surface, located at a normalized minor radius r/a = 0.6 – 0.7 at the mode onset.

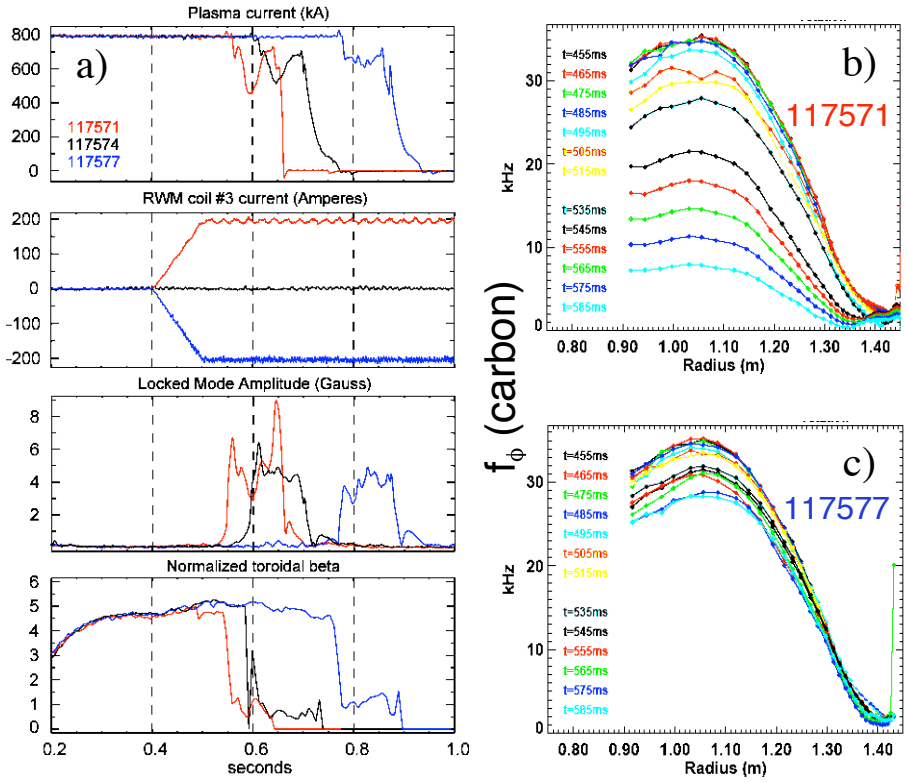

Fig. 7 a) Waveforms for similar discharges with no applied error-field correction and with an n=1 error field applied in both the augmenting and canceling directions with respect to the intrinsic field; b,c) Profiles of the toroidal rotation frequency (=$v_\phi/2\pi R$ measured by CHERS) at various times as the n=1 error field is applied in the augmenting (b) and canceling (c) directions.

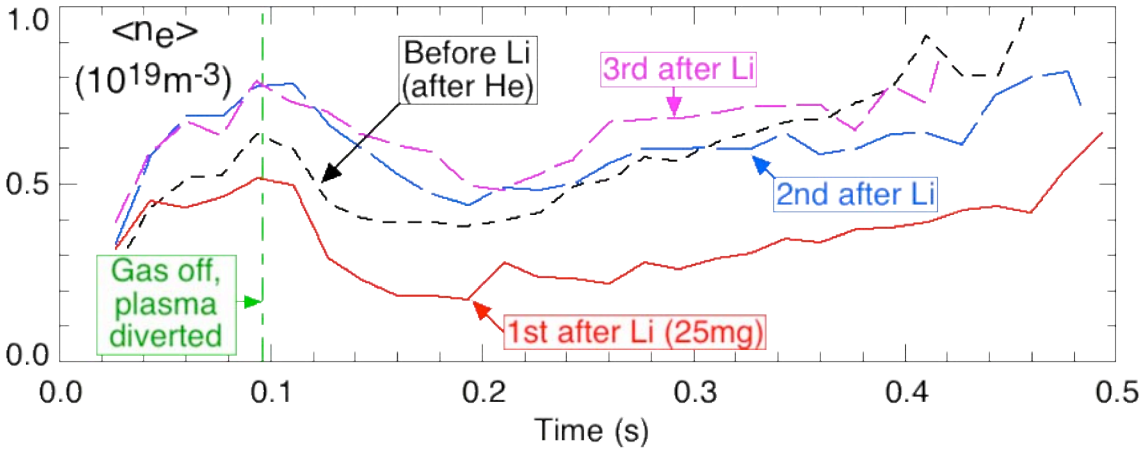

Fig. 8 Waveforms of the plasma volume average density (calculated from the Thomson scattering profiles) for a reference NBI-heated deuterium discharge before deposition of lithium on the plasma contact surfaces, and for the first three similar discharges after depositing 25mg of lithium in a series of helium ohmically heated plasmas.

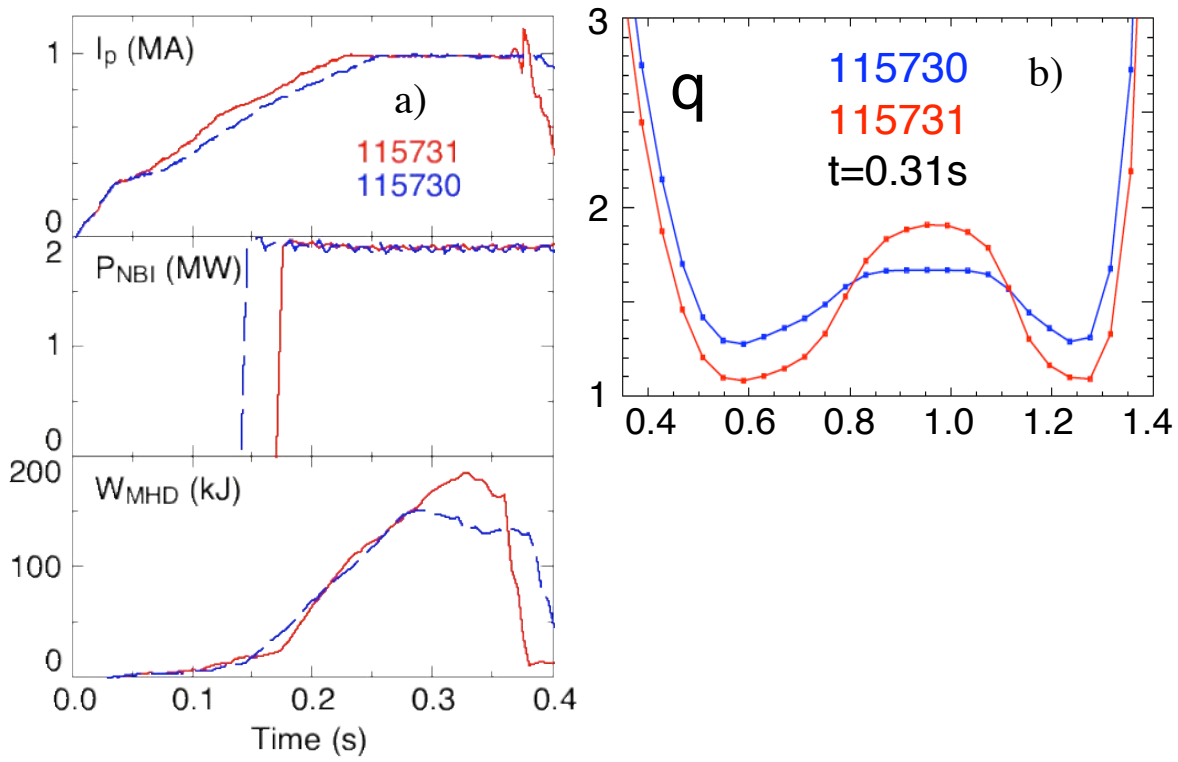

Fig. 9 a) Comparison of discharge waveforms for successive plasmas, the first developing a region of weakly, the second of strongly reversed shear; b) q-profiles for the two discharges at t = 0.31 s from analysis of the MSE data with the LRDFIT code.

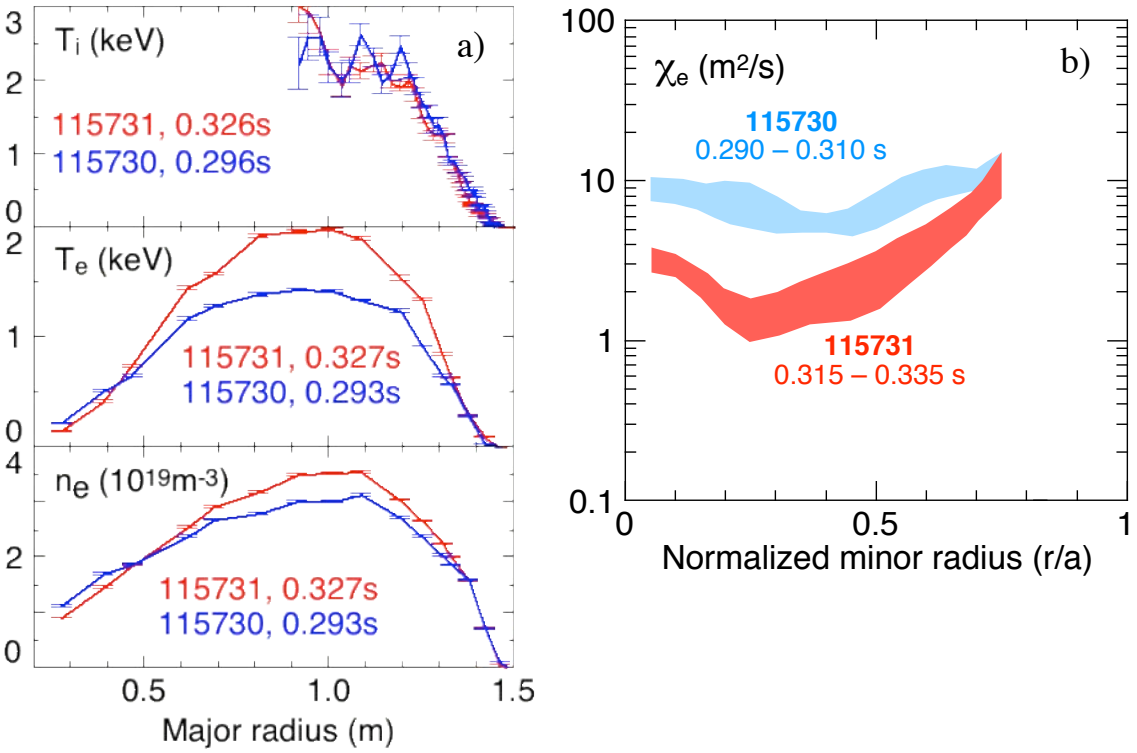

Fig. 10 a) Profiles of the plasma temperatures and density for the two discharges in Fig. 9 at the times of peak plasma energy; b) Profiles of the electron thermal diffusivity calculated by TRANSP (the bands indicate the variability of the diffusivity over the time interval indicated).

The Princeton Plasma Physics Laboratory is operated
by Princeton University under contract
with the U.S. Department of Energy.

Information Services
Princeton Plasma Physics Laboratory
P.O. Box 451
Princeton, NJ 08543

Phone: 609-243-2750
Fax: 609-243-2751
e-mail: pppl_info@pppl.gov
Internet Address: http://www.pppl.gov